

Modeling Vesicle Traffic Reveals Unexpected Consequences for Cdc42p-Mediated Polarity Establishment

Anita T. Layton,¹ Natasha S. Savage,² Audrey S. Howell,² Susheela Y. Carroll,³ David G. Drubin,³ and Daniel J. Lew^{2,*}

¹Department of Mathematics, Duke University, Durham, NC 27708, USA

²Department of Pharmacology and Cancer Biology, Duke University Medical Center, Durham, NC 27710, USA

³Department of Molecular and Cell Biology, University of California, Berkeley, Berkeley, CA 94720, USA

Summary

Background: Polarization in yeast has been proposed to involve a positive feedback loop whereby the polarity regulator Cdc42p orients actin cables, which deliver vesicles carrying Cdc42p to the polarization site. Previous mathematical models treating Cdc42p traffic as a membrane-free flux suggested that directed traffic would polarize Cdc42p, but it remained unclear whether Cdc42p would become polarized without the membrane-free simplifying assumption.

Results: We present mathematical models that explicitly consider stochastic vesicle traffic via exocytosis and endocytosis, providing several new insights. Our findings suggest that endocytic cargo influences the timing of vesicle internalization in yeast. Moreover, our models provide quantitative support for the view that integral membrane cargo proteins would become polarized by directed vesicle traffic given the experimentally determined rates of vesicle traffic and diffusion. However, such traffic cannot effectively polarize the more rapidly diffusing Cdc42p in the model without making additional assumptions that seem implausible and lack experimental support.

Conclusions: Our findings suggest that actin-directed vesicle traffic would perturb, rather than reinforce, polarization in yeast.

Introduction

Polarity establishment and maintenance are crucial to the function of many cell types. These processes are perhaps best understood in the budding yeast *Saccharomyces cerevisiae*, where genetic approaches identified a suite of polarity regulators centered on the conserved GTPase Cdc42p [1, 2]. Two positive feedback loops are thought to contribute to Cdc42p polarization in yeast. One is a Turing-type reaction-diffusion mechanism that can concentrate GTP-Cdc42p in a cytoskeleton-independent manner [3–5]. The other is a vesicle-recycling feedback loop whereby Cdc42p orients actin cables, which in turn deliver Cdc42p as cargo on secretory vesicles [6–8]. Here we address the requirements for such actin-mediated polarization.

The actin-mediated positive feedback hypothesis (Figure 1A) was first proposed to explain the spontaneous polarization of a GTP-locked mutant, Cdc42p^{Q61L}, when it was overexpressed in G1-arrested yeast cells [6]. This mutant cannot

employ the Turing mechanism, and Cdc42p^{Q61L} polarization is blocked by treatments that disrupt actin and/or exocytosis, consistent with the feedback hypothesis. However, disrupting actin or exocytosis would have many indirect consequences for cell physiology, potentially interfering with polarization even if the proposed actin-mediated feedback were not involved.

For actin-mediated feedback to operate, directed traffic of Cdc42p on vesicles must suffice to concentrate Cdc42p at the polarization site. A mathematical model incorporating polarized delivery, diffusion, and endocytic retrieval of Cdc42p (Figure 1B) indicated that once actin cables are polarized, traffic of Cdc42p should indeed generate and maintain a polarized distribution of Cdc42p at the plasma membrane [7, 9]. However, this model assumed that Cdc42p trafficking between internal pools and the plasma membrane can be treated as a simple protein flux, without considering the membranes that actually mediate the traffic. Using more realistic models with explicit vesicle traffic between the plasma membrane and an internal compartment, we now show that polarized vesicle delivery is incapable of maintaining a polarized distribution of cargo unless the cargo diffuses very slowly and is selectively concentrated into endocytic vesicles. Because Cdc42p is not thought to fit these criteria, our findings indicate a need to reevaluate the Cdc42p-actin feedback hypothesis.

Results

Assumptions of the Cdc42p Trafficking Model

The previous model considered the polarized distribution of Cdc42p in the plasma membrane to arise from delivery of Cdc42p to a specified window and subsequent retrieval of the protein by endocytosis before it diffused too far away (Figure 1B). The founding assumptions include:

- (1) All Cdc42p delivery is directed to a small patch (or “window”) in the plasma membrane.
- (2) Endocytosis is more active within the window (rate constant m) than it is outside the window (rate constant n).

These assumptions are reasonable because in a polarized cell, all detectable actin cables appear to be directed toward the polarization site, and the actin patches that mark sites of endocytosis are also concentrated near the polarization site [10, 11].

- (3) Cdc42p exocytosis occurs at a rate proportional to the amount of Cdc42p in the internal pool.
- (4) Cdc42p endocytosis from a given spot on the plasma membrane occurs at a rate proportional to the concentration of Cdc42p at that spot.

These are equivalent to assuming that Cdc42p is neither concentrated in nor excluded from exocytic and endocytic vesicles, so its rate of traffic is simply proportional to its concentration (surface density) at the donor membrane.

*Correspondence: daniel.lew@duke.edu

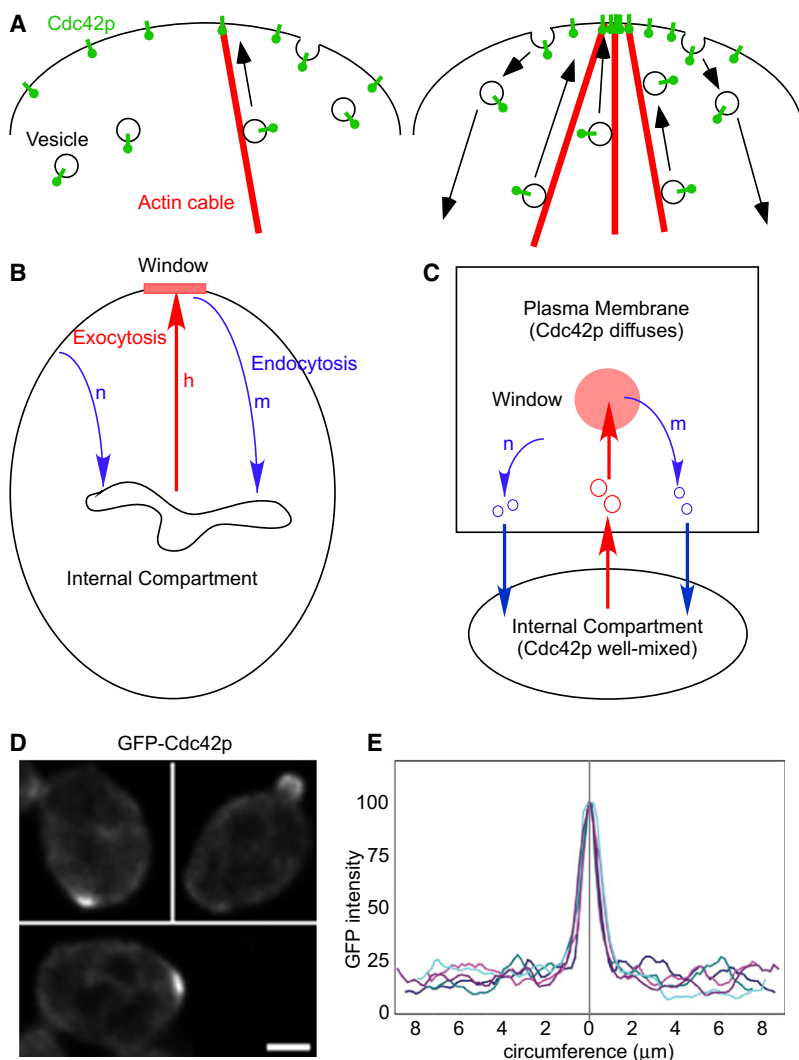


Figure 1. Models for Concentrating Cdc42p

(A) Left: Cdc42p can attach and orient actin cables, which deliver vesicles carrying Cdc42p to the plasma membrane. Right: the additional Cdc42p delivered by vesicles orients more actin cables, which deliver more vesicles with Cdc42p in a positive feedback loop.

(B) Previous mathematical models considered membrane-free Cdc42p fluxes to (rate constant h) and from (rate constants m or n) a 1D perimeter, which by rotational symmetry represents the 2D plasma membrane. All exocytic protein flux was directed to a polarization window, and endocytosis was more active in the window ($m > n$).

(C) We modeled Cdc42p fluxes as stochastic transfers of vesicles (red, large exocytic vesicles; blue, small endocytic vesicles) carrying Cdc42p between 2D plasma membrane and internal compartments. m and n now represent relative probabilities (per area) that endocytic vesicles form at different locations.

(D) Polarized distribution of GFP-Cdc42p in yeast. Scale bar represents $2 \mu\text{m}$.

(E) Line scans of GFP-Cdc42p in the plasma membrane of five polarized unbudded cells.

(6) Because the amount of membrane delivered by exocytosis equals that internalized by endocytosis, membrane traffic can be ignored and Cdc42p traffic can be treated as a direct protein flux to and from the plasma membrane.

This assumption yields a substantial simplification on the mathematical side: it allows one to describe stochastic delivery of vesicles (discrete membrane packets) carrying Cdc42p as a continuous simple flux. Consider, however, the effect of eliminating assumption 6 while retaining the others.

If Cdc42p traffics on vesicles, then it must be present at some specific concentration on those vesicles. Assumption 4 implies that the Cdc42p concentration on endocytic vesicles

This is reasonable given that no vesicular concentration or exclusion mechanisms are currently known for Cdc42p.

A potentially problematic issue is the question of how much of the intracellular Cdc42p pool is accessible for vesicular traffic. A prominent subpool of Cdc42p^{Q61L} resides on vacuole membranes, and a prominent subpool of endogenous Cdc42p is cytoplasmic (GDI-bound); both seem unlikely to be a direct source for exocytic Cdc42p. However, the assumptions may be valid if instead of treating the entire internal pool as a donor, we consider only a subpool of “transport-competent” Cdc42p in recycling endosomal and trans-Golgi membranes. The quantitative contribution of this pool to the total internal Cdc42p is unknown.

(5) The polarized cell is at steady state: Cdc42p delivery by exocytosis equals Cdc42p retrieval from the plasma membrane by endocytosis.

The steady-state assumption also applies to total plasma membrane area, which was assumed to be invariant. Because the cells are growing (implying net increase in the amounts of Cdc42p and membrane), this is clearly inaccurate over long periods. However, it is likely to apply over the short term.

is simply that of the Cdc42p at the source plasma membrane: we infer that the average Cdc42p concentration on endocytic vesicles will be intermediate between the maximum (peak) and minimum concentrations at the membrane. Assumption 5 (steady state) implies that the rate of exocytosis must equal the rate of endocytosis for both Cdc42p and membrane: we infer that the Cdc42p concentration on exocytic vesicles must equal the average Cdc42p concentration on endocytic vesicles. Therefore, the Cdc42p concentration on exocytic vesicles must be lower than the peak Cdc42p concentration at the plasma membrane, and delivery of new vesicles to that site would dilute the local Cdc42p rather than concentrate it. But then the peak concentration cannot be maintained at steady state. This argument suggests that without the simplifying assumption of membrane-free Cdc42p flux, the system would not in fact maintain a polarized steady state.

Explicit Modeling of Cdc42p Traffic by Exocytosis and Endocytosis

We set out to devise a model that incorporates the vesicular carriers. To model Cdc42p flux, we need to know the rate at which vesicles traffic in each direction, the spatial distribution of vesicle fission and fusion events, the concentration of

Table 1. Model Parameters

Parameter	Value	Comments	Reference
Plasma membrane area	78.5 μm^2	5 μm diameter sphere	diploid unbudded cell [7]
Polarization window area	0.785 μm^2	1 μm diameter circle	[7]
Exocytic vesicle area	0.0314 μm^2	0.1 μm diameter sphere	[36]
Endocytic vesicle area	0.00785 μm^2	0.05 μm diameter sphere	[37]
Frequency of exocytosis	0.42 vesicles/s	based on steady-state assumption	[7]
Frequency of endocytosis	1.67 vesicles/s	25 actin patches/cell and 15 s actin patch lifetime	[30, 38]
Ratio of endocytosis probabilities	40	probability/bin inside polarization window higher than outside	[7]
Area of internal compartment	55–78.5 μm^2	1 \times plasma membrane in bulk traffic model, 0.7 \times in sink models	see text
Cdc42p diffusion constant	0.036 $\mu\text{m}^2/\text{s}$		[7]
v-SNARE diffusion constant	0.0025 $\mu\text{m}^2/\text{s}$	assumed equal for pheromone receptor	[12]
Endocytic patch cargo trapping time τ	8 s	for uniform-time model	see text
Endocytic patch fill level	10	for uniform-fill model	see text
Maximum cargo-trapping time	24 s	for uniform-fill model	see text
Septin ring inner diameter	1 μm	surrounds polarization window	[45]
Septin ring outer diameter	1.6 μm		[45]

Cdc42p on the vesicles, and the membrane area of the vesicles. Some of this information is available in the literature; for the rest, we initially employed assumptions 1–5 above (Table 1). Vesicle traffic was modeled as the stochastic transfer of membrane packets carrying Cdc42p between a well-mixed internal compartment (representing the endomembrane system relevant to Cdc42p recycling) and the plasma membrane (Figure 1C). At the plasma membrane, traffic was directed to a central window, and Cdc42p distribution evolved as a result of both membrane traffic and diffusion. We call this the “bulk traffic” model, to indicate that vesicular Cdc42p concentration (surface density) is simply the concentration at the donor membrane that gave rise to the vesicle, and to distinguish it from subsequent models.

The Uniform Cdc42p Distribution Represents a Stable Steady State

A simulation initiated with equal Cdc42p concentration in the internal compartment and all over the plasma membrane remained unpolarized despite having all exocytosis directed to the window (Figure 2B). Because all vesicles carry the same concentration of Cdc42p as that on the plasma membrane, vesicle fusion and fission does not change the local Cdc42p concentration. Thus, the unpolarized state is stable despite highly polarized vesicle trafficking.

The stability of the unpolarized state in our model stands in marked contrast to the predictions of the previous model [7, 9]. In effect, that model had Cdc42p trafficking at infinite concentration, so that the local concentration of Cdc42p at the target membrane was always increased by the flux. By incorporating the vesicular carriers, our model allows for traffic to have no effect, or even to dilute Cdc42p, depending on the relation between the Cdc42p concentrations in the donor and target membranes.

The Polarized Cdc42p State Is Unstable and Decays to the Uniform Steady State

We next initiated simulations with Cdc42p at 10-fold higher concentration within the window than elsewhere (a distribution roughly similar to that in a polarized yeast cell; Figure 2A). This polarized distribution rapidly decayed to a uniform distribution (Figures 2C and 2D). Both exocytic and endocytic events collaborate with diffusion to dissipate polarity: endocytosis removes Cdc42p from the window, and fusion of exocytic vesicles dilutes Cdc42p in the window. The dissipative effect of

vesicle traffic is small compared with that of the diffusion coefficient estimated for Cdc42p ($D = 0.036 \mu\text{m}^2/\text{s}$; Figure 2E) [7] but quite large compared with that of the diffusion coefficient estimated for integral membrane proteins ($D = 0.0025 \mu\text{m}^2/\text{s}$; Figure 2F) [12]. Thus, a model incorporating vesicle traffic and adhering to assumptions 1–5 above cannot maintain a polarized state.

What If Cdc42p Were to Be Concentrated into Exocytic Vesicles?

In order to develop polarity in our model, a key requirement is that the concentration of Cdc42p in exocytic vesicles be higher than that at the peak of the Cdc42p distribution in the window. For as long as this holds true, each exocytic event should, at least transiently, increase polarity. Because the GFP-Cdc42p distribution does not reveal any internal compartment harboring Cdc42p at a concentration comparable to that in the window (Figure 1D), satisfying this condition requires that Cdc42p be more concentrated in the exocytic vesicles than it is in the internal compartment from which the vesicles emerge. Although not known to occur for Cdc42p, many integral membrane proteins do become more concentrated in vesicles compared to donor membranes (up to 10-fold, as estimated from electron microscopy of an abundant cargo protein targeted to the plasma membrane [13]). We next performed simulations in which Cdc42p was concentrated 10-fold during exocytic vesicle formation.

Starting from a homogeneous state, this new model did initially develop weak polarity (Figure 2G; first 2 min). However, the concentrated Cdc42p delivered by each exocytic vesicle dissipated rapidly, preventing robust polarization. Either increasing the vesicle trafficking rate (Figure 2H) or decreasing the diffusion constant (Figure 2I) enabled development of stronger polarity, implying that the inability to polarize effectively was due to an imbalance between slow vesicle trafficking and rapid diffusion.

On longer timescales (Figure 2J; 30 min), the polarizing effect of exocytosis was eliminated, resulting in a uniform distribution of Cdc42p. Although faster vesicle trafficking improved the initial polarization, polarity then dissipated rapidly (Figure 2K). Slowing diffusion was more effective (Figure 2L). The loss of polarity was due to a net transfer of Cdc42p from the internal compartment to the plasma membrane (Figure 2M). As Cdc42p became depleted from the internal compartment, exocytic vesicles carried less and less

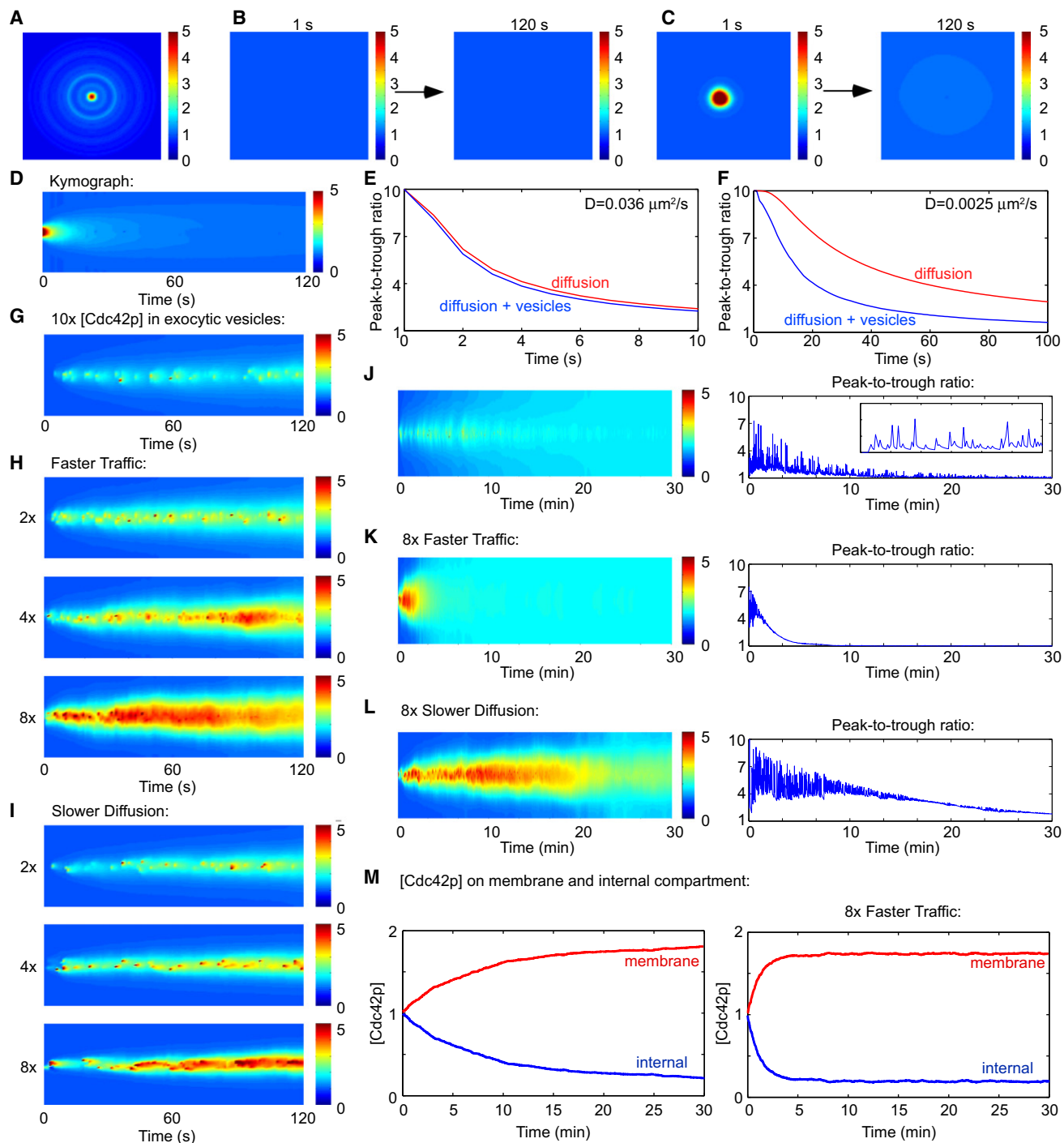


Figure 2. Directed Traffic of Cdc42p Cannot Sustain Polarization, Even If Cdc42p Is Concentrated into Exocytic Vesicles

(A) Cdc42p distribution from one of the cells in Figure 1E is displayed on a square plasma membrane by assuming rotational symmetry. Color bar indicates Cdc42p concentration in arbitrary units.

(B) The uniform Cdc42p distribution is stable. Left: Cdc42p distribution at $t = 1$ s. Right: Cdc42p distribution at $t = 120$ s.

(C) The polarized Cdc42p distribution is unstable. Left: Cdc42p distribution at $t = 1$ s. Right: Cdc42p distribution at $t = 120$ s.

(D) Kymograph of the simulation from (C) showing a slice through the middle of the plasma membrane (y axis) as time progresses (x axis).

(E) Plot of the peak-to-trough ratio of Cdc42p concentrations in the 2D plasma membrane from simulations performed as in (C). Red line indicates dissipation of the starting polarity by diffusion alone. Blue line indicates average of 20 simulations including vesicle traffic as well as diffusion. This dissipation rate is comparable to that of diffusion alone with $D = 0.04 \mu\text{m}^2/\text{s}$.

(F) As in (E), except that protein diffusion was modeled to be that of integral membrane proteins ($D = 0.0025 \mu\text{m}^2/\text{s}$). Here the dissipation with vesicle traffic is comparable to that of diffusion alone with $D = 0.008 \mu\text{m}^2/\text{s}$.

(G) Kymograph of a 120 s simulation in which Cdc42p is concentrated 10-fold from the internal compartment into exocytic vesicles.

(H) Simulations as in (G), but with 2-, 4-, or 8-fold faster vesicle traffic.

Cdc42p, reducing their polarizing effect. Meanwhile, Cdc42p accumulation at the plasma membrane made the gradient shallower. Faster vesicle trafficking accelerated the transfer of Cdc42p (Figure 2M), speeding the loss of polarity.

These simulations indicate that even if we alter the bulk traffic scenario to include a step that concentrates Cdc42p 10-fold during exocytic vesicle biogenesis, trafficking does not lead to a strong or sustained polarized state, for two reasons. First, there is a kinetic mismatch between the rate of vesicle traffic and the speed of Cdc42p diffusion, so that the polarizing effect of one vesicle is largely dissipated before the next vesicle arrives. Second, because Cdc42p is concentrated into exocytic but not endocytic vesicles, there is a net transfer of Cdc42p from the internal compartment to the plasma membrane. Once the relative amounts of Cdc42p in the two compartments reach steady state (with 10 times more Cdc42p on the plasma membrane than in the internal compartment), exocytic vesicles (though still 10-fold concentrated relative to what is left in the internal compartment) no longer carry enough Cdc42p to increase its concentration in the window. The situation is then equivalent to that of the bulk traffic model: all vesicles carry the same concentration of Cdc42p as that on the plasma membrane, and a polarized Cdc42p distribution rapidly decays to a uniform steady state.

What If Cdc42p Were to Be Concentrated into Endocytic Vesicles?

Could the problem discussed above be circumvented if Cdc42p were actively concentrated into endocytic vesicles as well as exocytic vesicles? Although not known to occur for Cdc42p, concentration of cargo in endocytic vesicles is well documented for many integral membrane proteins, thanks to a variety of “endocytosis signals” present in their cytoplasmic tails [14, 15]. Of particular interest are the vesicle-soluble NSF attachment protein receptors (v-SNAREs) that target fusion of exocytic vesicles with the plasma membrane. v-SNAREs are concentrated into both exocytic and endocytic vesicles, and in yeast, v-SNAREs exhibit a polarized distribution in the plasma membrane. Active endocytosis has been demonstrated to be essential for the polarized distribution of v-SNAREs, and appending a heterologous endocytosis signal to an otherwise unpolarized integral membrane protein causes it to become polarized [12]. Thus, we speculated that concentrating Cdc42p into endocytic (as well as exocytic) vesicles might allow the model to sustain a polarized steady state. We next develop such a model.

Modeling the Concentration of Endocytic Cargo Proteins into Patches

Because Cdc42p in the plasma membrane is not homogeneously distributed, the amount of Cdc42p present on a given endocytic vesicle will depend on the local Cdc42p concentration profile and the effectiveness with which Cdc42p becomes trapped in the forming vesicle. To develop a realistic model for this complex process, we began by considering the known cell

biology of endocytosis in yeast and deriving realistic parameters from well-characterized endocytic cargo.

The first step in vesicle biogenesis is the assembly of a coat containing clathrin and adaptor proteins at a patch on the plasma membrane. Accumulation of cargo into this patch then occurs via interactions between the specific endocytosis signals on the cargo and binding sites for those signals on adaptor proteins [15, 16]. After a variable time interval ($\sim 30\text{--}210$ s [17]), actin polymerization is initiated at the patch, and the membrane undergoes invagination and scission (a process taking ~ 15 s) to become an endocytic vesicle (Figure 3A).

We adapted our model for endocytosis to include cargo-trapping and internalization steps. For cargo trapping, we assume that for a time interval τ between patch formation and internalization, the patch acts as a diffusion sink: cargo can diffuse in but not out. For internalization, we introduce a 15 s “dead time,” during which the trapped cargo is insulated from the neighboring plasma membrane but has not yet been transferred to the internal compartment. Simulations of diffusion sink behavior starting from plasma membranes containing uniform concentrations of cargo indicated that the degree of cargo accumulation into a patch is approximately linear with τ (Figure 3B) and diffusion constant D (Figure 3C) in the relevant parameter range.

Modeling endocytic patch behavior also requires that we specify rules governing the switch between the cargo-trapping phase and the internalization phase of endocytosis: what is the trigger for actin polymerization? The answer to this question is not known. We considered two plausible hypotheses that led to distinct modeling strategies. (1) The switch is governed by a timer: formation of a patch starts a clock that promotes actin polymerization and internalization after some fixed τ (we call this the “uniform-time” model). (2) The switch is governed by patch cargo content: when this reaches a certain “fill level” f , actin polymerization and internalization occur (we call this the “uniform-fill” model). We note that in the uniform-fill model, the particular cargo under consideration stands in for the aggregate of all cargo proteins trapped by the patch. Moreover, the model parameters τ and f incorporate information on several unknown factors including the concentrations of adaptors, the efficiency of cargo trapping, and the patch lifetimes. A concern for the uniform-fill model, highlighted by preliminary simulations, is that patches forming in regions devoid of cargo could have extremely long lifetimes. To avoid such unphysiological effects, we included a provision that if a patch had failed to fill up by a designated maximum τ , it would go ahead and internalize with whatever cargo was present.

Parameter Estimation Based on Data from Unpolarized Cells

To assess what values of τ or f would accurately represent endocytosis for a well-characterized cargo, we simulated the internalization of pheromone/pheromone receptor complexes in unpolarized cells. With a diffusion constant

(I) Simulations as in (G), but with 2-, 4-, or 8-fold slower diffusion.

(J) Left: kymograph of a 30 min simulation started as in (G). Right: plot of the peak-to-trough ratio of Cdc42p concentrations in the 2D plasma membrane for the same simulation. Inset: first 2 min, showing that each vesicle fusion event yields a peak that dissipates rapidly.

(K) Simulation as in (J), but with 8-fold faster vesicle traffic.

(L) Simulation as in (J), but with 8-fold slower diffusion.

(M) Plot of average Cdc42p concentration on the plasma membrane (red line) and in the internal compartment (blue line) for the simulations shown in (J) (left) and (K) (right). Vesicle traffic mediates a net transfer of Cdc42p from the internal compartment to the plasma membrane, equilibrating when the membrane [Cdc42p] is 10 times the internal [Cdc42p].

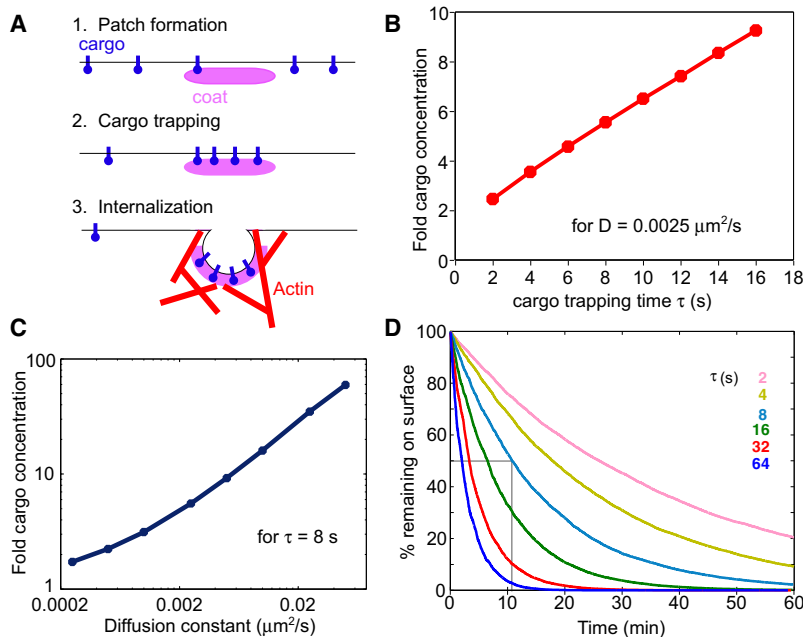


Figure 3. Simulating Endocytic Patches as Diffusion Sinks

(A) Schematic of endocytosis. (B) Simulations of cargo accumulation by diffusion sinks in unpolarized cells were used to assess the degree to which patches would concentrate a cargo with $D = 0.0025 \mu\text{m}^2/\text{s}$ in a given trapping time τ . (C) Simulations as in (B) were used to assess the degree to which patches would accumulate a cargo with varying diffusion constant in $\tau = 8 \text{ s}$. (D) Simulations of pheromone/receptor endocytosis assuming the indicated cargo trapping times (τ) for endocytic patches. The gray lines indicate that 50% of the cargo would be internalized in 11 min assuming $\tau = 8 \text{ s}$.

Behavior of Endocytic Patch Proteins in Polarized Cells Suggests that Cargo Triggers Internalization

Although both uniform-time and uniform-fill models yielded a polarized v-SNARE distribution, they differed in significant ways. With the uniform-time model, patches that formed in the window accumulated much more v-SNARE than those that formed at distant sites, so the amount of v-SNARE internalized

per patch was heterogeneous (Figure 4C). With the uniform-fill model, patches that formed in the window filled up much faster than those at distant sites, so patch τ was heterogeneous (Figure 4D). The two models yielded very different spatial distributions of patches engaged in cargo trapping (green in Figures 4E and 4F) versus internalization (red in Figures 4E and 4F). With the uniform-time model, the green/red patch ratio would be similar everywhere (Figure 4E), whereas with the uniform-fill model, the ratio would be significantly smaller near the window, where patches fill faster (Figure 4F).

per patch was heterogeneous (Figure 4C). With the uniform-fill model, patches that formed in the window filled up much faster than those at distant sites, so patch τ was heterogeneous (Figure 4D). The two models yielded very different spatial distributions of patches engaged in cargo trapping (green in Figures 4E and 4F) versus internalization (red in Figures 4E and 4F). With the uniform-time model, the green/red patch ratio would be similar everywhere (Figure 4E), whereas with the uniform-fill model, the ratio would be significantly smaller near the window, where patches fill faster (Figure 4F).

To distinguish between these models, we imaged yeast cells containing Ede1p-GFP, a marker of the cargo-trapping phase of endocytosis, and Abp1p-RFP, a marker of the internalization phase of endocytosis. In budded cells, all exocytic traffic is directed to the bud (analogous to the central window in the simulations), and the distribution of marker proteins dramatically supported the uniform-fill model: the Ede1p-GFP/Abp1p-RFP ratio was much smaller in buds than in mothers (Figure 4G). Direct examination of patch lifetimes showed that whereas Abp1p patches displayed uniform 13–14 s lifetimes, Ede1p patches were longer lived in mothers than in buds of polarized cells (Figure 4H, upper inset). Measurement of patch lifetimes requires that the entire patch lifetime be included in a movie, so the data used to calculate these averages excluded many Ede1p patches that did not internalize by the end of our 4 min movies and therefore underestimate the true Ede1p patch lifetime in mother cells. Indeed, we observed a significant number of Ede1p patches in polarized mother cells that persisted for the entire duration of the movies: inclusion of these patches yielded the lifetime distributions shown in Figure 4H (top). Once cells progressed to the mature bud stage where secretion of cargo was unpolarized, Ede1p patch lifetimes were similar in mothers and buds, and very long-lived patches were no longer detected (Figure 4H, bottom). We conclude that the uniform-fill model better represents the situation in yeast, suggesting that cargo filling can trigger endocytic patch internalization.

Polarized Traffic of a v-SNARE Yields a Polarized Steady State

To assess whether polarized traffic would generate a polarized v-SNARE distribution in our model, we conducted simulations with 10-fold concentration of cargo into exocytic vesicles and with endocytosis occurring using either the uniform-time model with $\tau = 8 \text{ s}$ (Figure 4A) or the uniform-fill model with $f = 10$ (Figure 4B). Vesicle trafficking frequencies and spatial distributions were as in the bulk traffic model. We started with the uniform steady state resulting from simulated traffic in unpolarized cells and switched to polarized traffic. Both models rapidly generated a highly polarized state with a broad peak in protein concentration that was maintained for >1 hr. Thus, unlike a bulk cargo, a protein with the trafficking characteristics of a v-SNARE would become polarized by directed traffic.

for integral membrane proteins of $0.0025 \mu\text{m}^2/\text{s}$ [12], simulations yielded the kinetics of pheromone/receptor internalization shown in Figure 3D. Experimental determinations suggest $t_{1/2}$ values of 6–13 min [18–22], corresponding to τ values of 6–16 s (Figure 3D), based on which we selected a value of $\tau = 8 \text{ s}$. With this τ , integral membrane endocytic cargo proteins would be concentrated ~ 6 -fold into the patch (Figures 3B and 3C). Comparable pheromone internalization kinetics are predicted by the uniform-fill model with $f = 10$.

Cargo recycled between the plasma membrane and the internal compartment would, in unpolarized cells, reach a steady-state distribution reflecting the relative degree to which it gets concentrated into exocytic and endocytic vesicles. If cargo is concentrated 10-fold in exocytic vesicles and 6-fold in endocytic vesicles, a recycling protein would reach a steady state in which the cargo concentration in the internal compartment was 60% of that on the plasma membrane. This is in reasonable agreement with the visual impression from images of either GFP-Cdc42p (Figure 1D) or v-SNARE [23, 24] distribution in yeast.

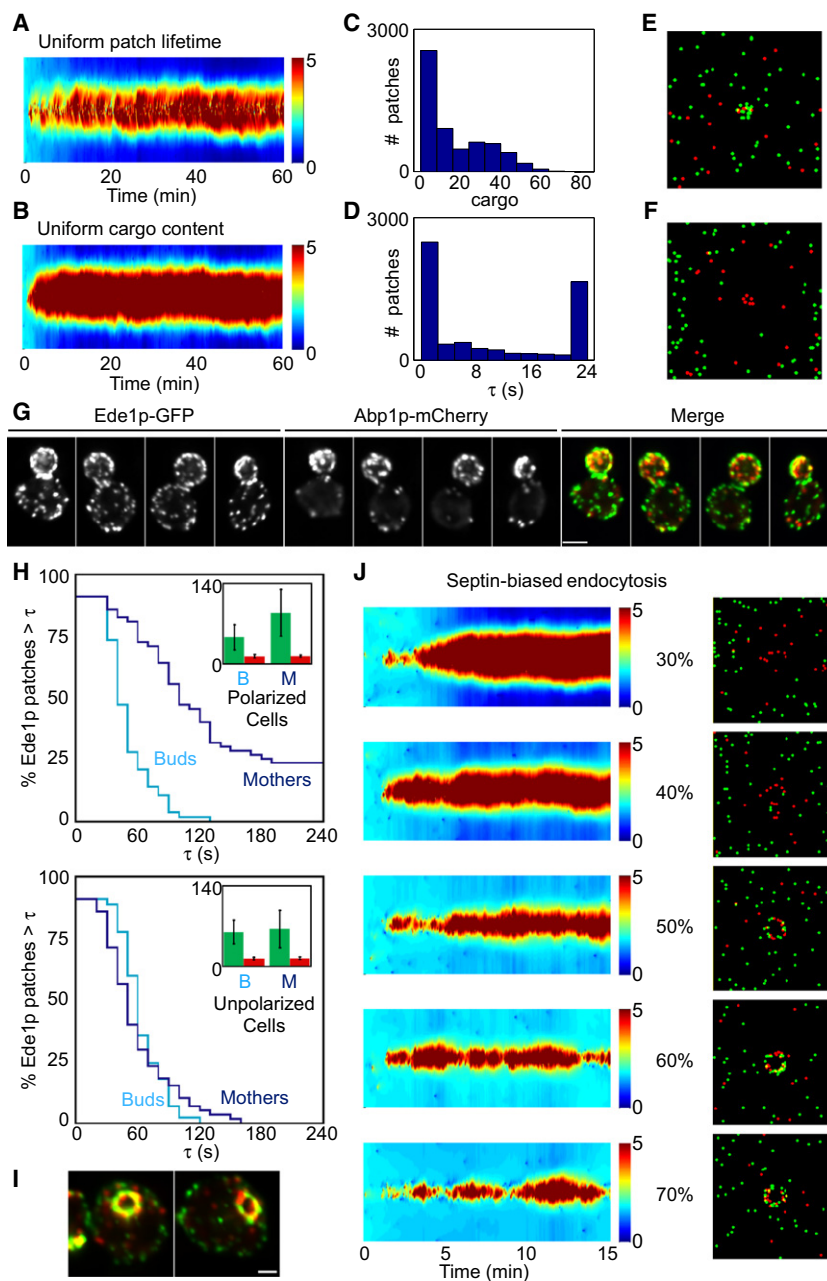


Figure 4. Polarization of v-SNAREs by Vesicle Traffic Simulations were performed using uniform-time (A, C, and E) or uniform-fill (B, D, and F) models.

(A and B) Starting from the unpolarized steady state, model cells were switched to polarized traffic at 1 min and simulated for 1 hr. Kymographs show that both models developed and sustained a polarized cargo distribution.

(C) Histogram showing amount of cargo internalized per patch in a uniform-time simulation.

(D) Histogram showing patch τ in a uniform-fill simulation.

(E and F) Snapshots of endocytic patch distributions in uniform-time (E) or uniform-fill (F) simulations. Green indicates patches during cargo-trapping phase; red indicates patches during internalization phase.

(G and I) Micrographs of cells harboring the patch markers Ede1p-GFP (green) and Abp1p-mCherry (red).

(G) Budded cells show more red than green patches in the bud but more green than red patches in the mother. Scale bar represents 2 μm .

(H) Ede1p and Abp1p patch lifetimes in mothers and buds. Main graphs: Ede1p-GFP lifetimes. x axis shows time τ ; y axis shows percent of patches with lifetimes longer than τ . Data were binned in 10 s increments. $n = 40\text{--}55$ patches in each data set, from 4 min movies. Polarized (upper panel) and unpolarized (bottom panel) cells were distinguished by monitoring Abp1p-RFP distribution. All cells were medium to large budded. Inset: average (\pm standard deviation) patch lifetimes for Ede1p-GFP (green) and Abp1p-RFP (red) in buds (B) and mothers (M).

(I) Unbudded polarized cells show a ring of patches surrounding the polarization site. Scale bar represents 1 μm .

(J) Simulations as in (B) (uniform cargo content), but with endocytosis biased toward the septin ring rather than the central window. Left: kymographs of cargo distribution. Right: snapshots of endocytic patch distributions. Each row is a different simulation assuming that the indicated fraction (30%–70%) of patches formed within the ring. The ring has inner diameter 1 μm and outer diameter 1.6 μm and is most clearly seen by looking at patch locations in the high-bias (70%) simulations.

Septin-Mediated Targeting of Endocytosis Sculpts the Polarized Protein Distribution

Figure 4G also confirms previous studies indicating that patches tend to cluster at the mother-bud neck. Because of their close packing, it has not been possible to confirm that the patches at the neck behave in the same stereotyped manner as those elsewhere, but here we assume that they do. Neck localization is due to the influence of the septins, a family of cytoskeletal polymers that assemble in a ring surrounding the polarization site and at the neck [17, 25, 26]. Unbudded but polarized cells (Figure 4I) also displayed patches clustered in a ring (rather than uniformly within the window as assumed in previous models), consistent with a major influence of septins on patch placement. To incorporate these findings, we changed the spatial probability distribution for endocytosis in the model to bias patch formation

to a ring surrounding the window. Simulations using the uniform-fill model in which increasing numbers of patches formed within the ring produced increasingly narrow polarized v-SNARE distributions in the plasma membrane (Figure 4J). Thus, septin-biased endocytosis has the potential to sculpt the polarized distribution of recycling cargo proteins in the plasma membrane.

Could Active Endocytosis Polarize Cdc42p?

Returning to the question of Cdc42p polarization, does the successful polarization of a v-SNARE in our models (Figure 4) imply that Cdc42p could be similarly polarized if it were also to be concentrated into endocytic as well as exocytic vesicles? The v-SNARE diffusion constant (0.0025 $\mu\text{m}^2/\text{s}$) [12] is much slower than that estimated for Cdc42p (0.036 $\mu\text{m}^2/\text{s}$) [7]. To model Cdc42p behavior, we added a “passenger” cargo to the v-SNARE uniform-fill model with 50% septin-biased endocytosis. The passenger, Cdc42p, is carried by the same

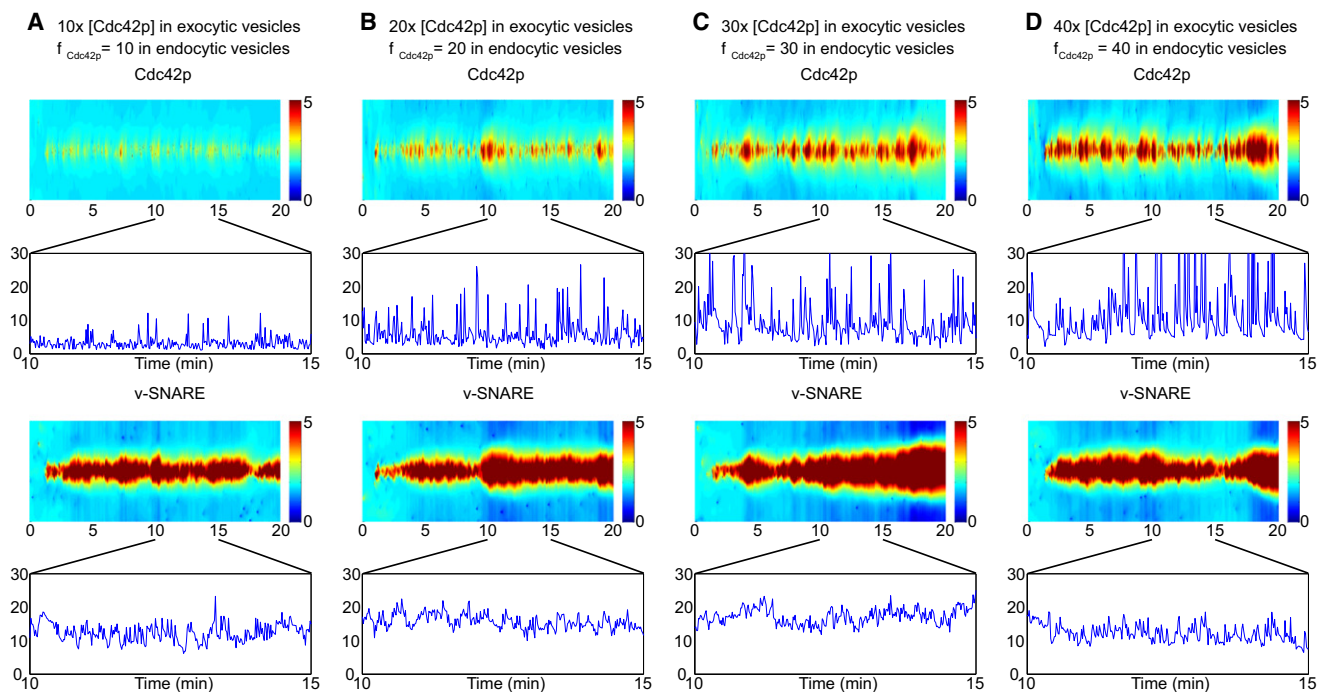


Figure 5. Simulating Traffic of Vesicles Carrying Both v-SNAREs and Cdc42p

Simulations were performed assuming a uniform cargo content with 50% septin-biased patches as in Figure 4J. In addition to v-SNARE cargo, a more rapidly diffusing “passenger” cargo representing Cdc42p traffics on the same vesicles. The fold concentration of Cdc42p into exocytic vesicles and the Cdc42p fill level f_{Cdc42p} were set to 10 (same as for v-SNARE) in (A), 20 in (B), 30 in (C), and 40 in (D). Upper panels: kymographs of Cdc42p distribution during 20 min simulation and plots showing the [Cdc42p] peak-to-trough ratio during an interval between 10 and 15 min. Lower panels: kymographs of v-SNARE distribution for the same simulation and plots showing the [v-SNARE] peak-to-trough ratio in the same interval.

vesicles as the v-SNARE but does not affect the timing of vesicle internalization. This strategy allows independent control of the degree to which Cdc42p becomes concentrated into exocytic and endocytic vesicles. For the latter, we specify a Cdc42p “fill level” f_{Cdc42p} that reflects factors such as the trapping efficiency and total capacity of endocytic patches for Cdc42p.

Simulations with this “dual-cargo” model showed that if Cdc42p were to be concentrated into exocytic and endocytic vesicles to the same extent as v-SNAREs ($f = 10$), the rapid diffusion of Cdc42p would dissipate the polarity created by vesicle traffic (Figure 5A). Although a polarized distribution could be produced by further increasing the vesicular Cdc42p concentration ($f_{\text{Cdc42p}} = 30-40$), such polarization displayed dramatic fluctuations in Cdc42p distribution (Figures 5B–5D). Filming of GFP-Cdc42p [8] has not revealed the bright spots or extreme fluctuations predicted by this model. Thus, given the quantitative constraints on vesicle trafficking frequencies and the published Cdc42p diffusion constant, Cdc42p could not be effectively polarized via trafficking.

Discussion

Effect of Cdc42p Traffic on Polarization

Polarity establishment in yeast is thought to involve a positive feedback loop in which Cdc42p is delivered to the polarization site by vesicles traveling along actin cables, which themselves are oriented by Cdc42p. Previous mathematical models treated Cdc42p traffic as a direct protein flux, without taking into consideration the membranes that actually carry the Cdc42p. In such models, all traffic concentrates Cdc42p at

the target membrane. Realistically, however, vesicle fusion would only concentrate Cdc42p if the Cdc42p concentration on the vesicle were higher than that in the target membrane. We present models of Cdc42p traffic that explicitly consider the vesicular carriers and show that bulk traffic of Cdc42p would dissipate, not enhance, polarity (Figure 2).

Our simulations suggest that in contrast to bulk cargo, an integral membrane cargo protein that diffuses slowly and is actively concentrated into both exocytic and endocytic vesicles would become effectively polarized (Figure 4). The key parameters in these models (vesicle dimensions and trafficking frequencies, degree of cargo trapping into endocytic patches, and diffusion constant) are all constrained within a factor of ~ 2 by experimental data, so the ability of the models to reproduce the experimentally observed v-SNARE distribution provides strong quantitative support for the prevailing hypothesis that v-SNARE polarization is due to polarized vesicle traffic [12].

In budded cells, v-SNAREs are concentrated in the bud and largely absent from the mother plasma membrane [12]. One possible basis for this is a diffusion barrier at the mother-bud neck. Indeed, the septin ring, which localizes to the neck, is thought to create such a barrier [27]. Recent studies suggested that the septin ring might also promote endocytic patch formation [17, 25]. We modeled the effect of septin-biased endocytosis on the distribution of cargo in the plasma membrane and found that when vesicle delivery to a central window is coupled with a sufficient septin bias of endocytosis around the window, recycling cargo proteins are restricted to the vicinity of the window. This effect provides an alternative explanation for why v-SNAREs and similar cargo proteins are

restricted to the bud. Moreover, like septin-restricted diffusion, it would also keep such proteins focused near the polarization site in unbudded cells.

We recently generated a yeast strain that was synthetically rewired by fusing a normally cytoplasmic polarity protein to a v-SNARE [28]. The ability of this rewired strain, in which actin-independent polarization was disabled, to develop polarity suggests that actin-mediated vesicle traffic can concentrate a polarity protein with the trafficking characteristics of a v-SNARE to a sufficient degree to enable positive feedback. Together, the rewired strain and the models developed here support the idea that an actin-mediated positive feedback loop can operate successfully if a polarity protein has suitable trafficking characteristics.

Do any endogenous polarity proteins exhibit these characteristics? None of the known polarity proteins in yeast are integral membrane proteins, and there is as yet no evidence to indicate that any can be actively endocytosed. Most polarity regulators are cytoplasmic proteins that associate only transiently with the plasma membrane, and although Cdc42p itself is a peripheral membrane protein, it is thought to diffuse quite rapidly relative to v-SNAREs. We show that vesicle traffic would be ineffective in polarizing such rapidly diffusing proteins even if they did become concentrated in forming vesicles.

Cdc42p and other polarity regulators become polarized even in the complete absence of polymerized actin in yeast [3, 29], so it is clear that actin-independent polarization mechanisms exist. Actin-independent polarization is suggested to operate via a positive feedback loop in which GTP-Cdc42p recruits a rapidly diffusing cytoplasmic complex containing the Cdc42p-directed GEF, which then promotes GTP loading of neighboring Cdc42p [4]. This system acts via a Turing-type reaction-diffusion mechanism [5] and in principle suffices to account for polarity establishment in yeast.

New Insights from Modeling Endocytosis

Endocytic patches form at the plasma membrane, stay there (presumably trapping cargo) for a time, and then internalize in a stereotypical sequence [30]. We developed two models for cargo endocytosis: one assumed that patch lifetime is uniform, whereas the other assumed that patch cargo content is uniform (i.e., patches are triggered to internalize once they trap a certain amount of cargo). The models behaved similarly in unpolarized cells, but they differed in significant ways in polarized cells. In particular, if patches are triggered to internalize once they trap a certain amount of cargo, then patch lifetimes should be much shorter in the bud (where abundant cargo rapidly fills the patch) than in the mother. Using markers of the cargo-trapping and internalization phases of endocytosis, we confirmed this prediction, suggesting that endocytic cargo can promote internalization.

How would cargo trigger internalization? Internalization is initiated by Arp2/3-mediated actin polymerization [31], and some endocytic cargo adaptors can inhibit Arp2/3 [32, 33]. We speculate that cargo binding to the adaptors might relieve their inhibition of Arp2/3, enabling internalization once sufficient cargo binding occurs.

In mammalian cells, cargo is thought to bias clathrin patch biogenesis toward productive coated-pit formation as opposed to abortive disassembly [34, 35], but abortive events have not been described in yeast. Why would cargo influence patch internalization instead of initial maturation in yeast? One possibility is suggested by the observation that membrane

proteins diffuse much more slowly in the yeast plasma membrane than in mammalian plasma membranes [12]. With slow cargo diffusion, a longer time would be required for yeast clathrin patches to assess the local cargo environment. Regulation of a later step in the endocytic process may allow sufficient time for accurate cargo monitoring, yielding a more effective strategy to couple cargo abundance with internalization.

Conclusions

Explicit modeling of vesicular traffic reveals unappreciated issues that question the validity of the widely accepted Cdc42p-actin-vesicle positive feedback loop. Our models suggest that to exploit positive feedback, a polarity regulator would have to diffuse very slowly and be concentrated into both exocytic and endocytic vesicles. At present, these features are not known to apply to any yeast polarity regulators. The modeling results should stimulate future studies to determine whether polarity regulators with these characteristics exist. If they do not, then our findings suggest that vesicle traffic would act to dissipate, not reinforce, polarization.

Experimental Procedures

Simulating Bulk Traffic of Cdc42p

Simulations were performed with MATLAB using the program `bulkcargo.m`, which models vesicle trafficking between an internal compartment and the plasma membrane (all programs are provided in the [Supplemental Information](#); for parameter values, see [Table 1](#)).

The Plasma Membrane

We represented the plasma membrane of an unbudded diploid cell as a square grid of 10,000 bins. Each bin contains Cdc42p at a concentration that evolves with time as a result of diffusion, exocytosis, and endocytosis. To avoid edge effects, we diffusionally connected the right and left edges of the grid as well as the top and bottom edges.

The Intracellular Compartment

As in previous work, we considered the entire endomembrane system relevant to Cdc42p recycling as a single well-mixed compartment. We set the area of this compartment equal to that of the plasma membrane.

The Vesicles

Electron microscopy suggests a secretory vesicle diameter of ~ 100 nm [36] and an endocytic vesicle diameter of ~ 50 nm [37], with areas corresponding to four bins and one bin of the plasma membrane, respectively.

Exocytosis

Exocytic events were modeled as instantaneous transfers of membrane and Cdc42p from the internal compartment to the plasma membrane: a fusion site on the plasma membrane was chosen (see below), and four (2×2) bins were “inserted.” Because adding bins to the plasma membrane would make diffusion difficult to model, we instead resized all bins to account for the increased area. We redistributed the Cdc42p as follows: for the four “inserted” bins, the Cdc42p concentration was reset to be equal to the Cdc42p concentration in the internal compartment. The pre-exocytosis plasma membrane was assumed to stretch radially, with the center of the four “inserted” bins as the origin. The Cdc42p in the (10,000 – 4) bins that correspond to the pre-exocytosis plasma membrane was recomputed using a spatial interpolation algorithm that preserves the preexisting Cdc42p distribution around the insertion site and conserves the total amount of Cdc42p (see [Supplemental Results and Discussion](#) for further discussion of interpolation). The area and Cdc42p content of the internal compartment were also adjusted to deduct the amount inserted into the plasma membrane.

Endocytosis

Endocytic events were modeled as instantaneous transfers of membrane and Cdc42p from the plasma membrane to the internal compartment: a single bin on the plasma membrane was chosen to endocytose (see below), and its membrane and Cdc42p content was removed from the plasma membrane and added to the internal compartment. We resized plasma membrane bins to account for the reduced total area and redistributed the Cdc42p by radial interpolation, maintaining the preexisting Cdc42p distribution but deducting the endocytosed amount.

Frequency of Endocytosis

Endocytic events are marked by transient accumulation of F-actin in an actin patch with a stereotypical lifetime of ~ 15 s [31], and an unpolarized cell of diameter $\sim 5 \mu\text{m}$ has ~ 25 actin patches at any given time [38], suggesting that endocytic events occur at a rate of $\sim 25/15$ or 1.67/s. To a first approximation, we assumed that they occur with similar frequency in polarized cells.

Frequency of Exocytosis

Given that exocytic vesicles have four times the surface area of endocytic vesicles, exocytosis must occur at 4-fold lower frequency to maintain a steady state.

The Polarization Window

We modeled the window as an $\sim 1 \mu\text{m}$ diameter circular zone in the center of the plasma membrane [7].

Spatial Probability Distribution for Exocytosis

To simulate unpolarized cells, we assumed a uniform probability (1/10,000) that any given bin is chosen as the exocytosis site. To simulate polarized cells, we assumed that exocytosis occurs with uniform probability at any bin within the window and does not occur elsewhere.

Spatial Probability Distribution for Endocytosis

To simulate unpolarized cells, we assumed a uniform probability that any given bin is chosen as the endocytosis site. To simulate polarized cells, we assumed that endocytosis occurs with a higher (uniform) probability within the window and a lower probability elsewhere. Using $m/n = 40$ and a $1 \mu\text{m}$ diameter window [7], $\sim 29\%$ of all endocytic events occurred in the window.

Diffusion

The diffusion constant for Cdc42p in the yeast plasma membrane is reported to be $0.036 \mu\text{m}^2/\text{s}$ [7]. In between exocytic and endocytic events, we allowed diffusion to occur between neighboring bins in the plasma membrane, using the backward Euler method to advance Cdc42p in time.

Simulating Cargo Concentration into Exocytic Vesicles

Simulations were performed using the program *exoconc.m*, which is identical to the bulk cargo model except that exocytic events insert four bins into the plasma membrane with 10 times the cargo concentration present in the internal compartment, and the corresponding amount of cargo is subtracted from the internal compartment.

Simulating Cargo Concentration into Endocytic Vesicles

Simulations were performed using the program *fixedlivesink.m* for the uniform-time model and *fillsink.m* for the uniform-fill model. With the exceptions noted below, the models are similar to the *exoconc.m* model above.

Endocytic Patches as Diffusion Sinks

We assumed that cargo can diffuse into a bin designated as an endocytosis site but cannot diffuse out. A problem in accurately modeling the diffusion sink is that, because the cargo concentration in the sink may be substantially higher than in the neighboring bins, the radial interpolation algorithms we use to redistribute cargo following vesicle fusion and fission events have the potential to artificially “move” cargo into or out of the sink. To avoid this complication, we excluded the “sink” bins from the interpolation process.

[³⁵S]Pheromone Internalization

Simulations were initiated with uniform cargo concentration on the plasma membrane and no cargo in the internal compartment. Endocytic events transferred membrane but not cargo, to model the fact that labeled pheromone would be destroyed, not recycled.

v-SNARE Recycling in Unpolarized Cells

Exocytic vesicles were assumed to concentrate cargo 10-fold, and (for $\tau = 8$ s, $D = 0.0025 \mu\text{m}^2/\text{s}$) endocytic vesicles would concentrate cargo ~ 6 -fold, so that at steady state, the internal compartment had a concentration 60% of that on the plasma membrane. To accommodate experimental findings suggesting that $\sim 30\%$ of the total v-SNARE is internal at steady state [24], we set the size (area) of the internal compartment to be 70% that of the plasma membrane. The unpolarized steady state was then used as a starting point for simulations of polarized traffic.

Septin-Biased Endocytosis

We designated a septin ring zone as an annulus surrounding the central window (inner diameter $1 \mu\text{m}$, outer diameter $1.6 \mu\text{m}$). Simulations specified the probability that a given endocytic patch would (as a result of septin bias) form inside the ring (Figure 4J). Septin-biased patches occur with uniform probability at any bin within the ring, and other patches occur with uniform probability anywhere.

Cdc42p as a Passenger Cargo

We simulated v-SNARE traffic with the uniform-fill model and 50% septin-biased endocytosis but added a second cargo with $D = 0.036 \mu\text{m}^2/\text{s}$ to represent Cdc42p. Each vesicle carries both Cdc42p and v-SNARE, but only the v-SNARE influences the timing of internalization: if Cdc42p reaches its fill level first, then no further Cdc42p trapping occurs; if v-SNARE reaches its fill level first, then whatever amount of Cdc42p has accumulated at that point is internalized.

Yeast Strains

The yeast strains used in this study were in the YEF473 background (*his3- Δ 200 leu2- Δ 1 lys2-801 trp1- Δ 63 ura3-52*). The *rsr1::TRP1*, *ABP1-mCherry:Kan^R* [28], *cdc42::HIS3*, and *GFP-CDC42:URA3* [39] alleles have been described previously. *EDE1-GFP* was generated using the PCR-based C-terminal tagging method [40]. *DLY12709 (MATa/ α .cdc42::HIS3/CDC42 GFP-CDC42:URA3/URA3 rsr1::TRP1/RSR1)* was imaged for Figure 1, and *DLY12452 (MATa EDE1-GFP:Kan^R ABP1-mCherry:Kan^R rsr1::TRP1)* was imaged for Figures 4G and 4I. For Figure 4H, *DDY3868 (MATa EDE1-GFP::HIS3 ABP1-RFP::HIS3)* was used to determine Ede1p patch lifetimes [17], and *DDY3058 (MATa ABP1-RFP::HIS3)* was used to calculate Abp1p patch lifetimes [41].

Live-Cell Imaging and Image Analysis

Cells growing exponentially in 2% dextrose complete synthetic medium were mounted on a slide with a slab of medium solidified with 2% agarose (Denville Scientific). Images were acquired using an Axio Observer.Z1 (Carl Zeiss) with a $100\times/1.47$ Plan Apochromat oil-immersion objective and the stage incubator set at 30°C . Images were captured with either a QuantEM EM-CCD camera (Figure 1) (Princeton Instruments) or a CoolSNAP ES2 CCD camera (Figure 4) (Photometrics) controlled by MetaMorph software (Universal Imaging). All cells were imaged for fluorescence and differential interference contrast with z planes at $0.24 \mu\text{m}$ step size.

Image deconvolution was performed with Huygens Essential software (Scientific Volume Imaging) using the classic maximum-likelihood estimation and predicted point-spread function. The line scans in Figure 1E were generated using MetaMorph from the average intensity of a two-pixel-wide line drawn around the periphery of an unbudded cell in the single deconvolved z plane with the peak polarized intensity. The images in Figure 4 are maximum-intensity projections of 30 deconvolved z planes. Images were prepared for presentation using Adobe Photoshop.

We used different microscopy methods to monitor Ede1p and Abp1p patch lifetimes. Abp1p patches are short lived, so patch lifetime could be assessed accurately by taking short (90 s) movies at high temporal resolution (1 frame/s) imaging a medial focal plane with an Olympus IX71 microscope. Images were processed using ImageJ (<http://rsbweb.nih.gov/ij/index.html>) before analysis. Because Ede1p patches are more abundant and longer lived, it is difficult to resolve the crowded patches using this approach, and longer movies are necessary to capture Ede1p lifetimes. Thus, we imaged the top surface of the cells using near-total internal reflection fluorescence microscopy (near-TIRFM) to clearly distinguish individual patches and took longer (4 min) movies at lower temporal resolution (1 frame/2 s) to reduce photobleaching. Near-TIRFM is similar to TIRFM [42], except that the angle of incidence is decreased in order to increase the illumination depth beyond the evanescent wave [43, 44]. This method better illuminates the plasma membrane through the yeast cell wall. Yeast were grown to log phase in synthetic medium lacking tryptophan and immobilized on concanavalin A-coated coverslips (Olympus). An Olympus IX81 microscope was used for simultaneous two-color TIRF microscopy of cells expressing Ede1p-GFP and Abp1p-RFP, as described in [17]. Polarization of the cells was assessed by the distribution of Abp1p-RFP patches visualized in the red channel.

Supplemental Information

Supplemental Information includes Supplemental Results and Discussion, five figures, and Supplemental Experimental Procedures and can be found with this article online at doi:10.1016/j.cub.2011.01.012.

Acknowledgments

We thank Nick Buchler, Pat Brennwald, Tim Elston, Meng Jin, Mike Reed, Dan Kiehart, and members of the Lew laboratory for stimulating discussions and comments on the manuscript. We also thank Trevin Zyla for assistance with strain construction. This work was supported by National Science

Foundation grant DMS-0701412 to A.T.L. and National Institutes of Health grants GM62300 to D.J.L. and GM50399 to D.G.D.

Received: October 25, 2010

Revised: December 30, 2010

Accepted: January 5, 2011

Published online: January 27, 2011

References

- Pringle, J.R., Bi, E., Harkins, H.A., Zahner, J.E., De Virgilio, C., Chant, J., Corrado, K., and Fares, H. (1995). Establishment of cell polarity in yeast. *Cold Spring Harb. Symp. Quant. Biol.* **60**, 729–744.
- Park, H.O., and Bi, E. (2007). Central roles of small GTPases in the development of cell polarity in yeast and beyond. *Microbiol. Mol. Biol. Rev.* **71**, 48–96.
- Irazaqui, J.E., Gladfelter, A.S., and Lew, D.J. (2003). Scaffold-mediated symmetry breaking by Cdc42p. *Nat. Cell Biol.* **5**, 1062–1070.
- Kozubowski, L., Saito, K., Johnson, J.M., Howell, A.S., Zyla, T.R., and Lew, D.J. (2008). Symmetry-breaking polarization driven by a Cdc42p GEF-PAK complex. *Curr. Biol.* **18**, 1719–1726.
- Goryachev, A.B., and Pokhilko, A.V. (2008). Dynamics of Cdc42 network embodies a Turing-type mechanism of yeast cell polarity. *FEBS Lett.* **582**, 1437–1443.
- Wedlich-Soldner, R., Altschuler, S., Wu, L., and Li, R. (2003). Spontaneous cell polarization through actomyosin-based delivery of the Cdc42 GTPase. *Science* **299**, 1231–1235.
- Marco, E., Wedlich-Soldner, R., Li, R., Altschuler, S.J., and Wu, L.F. (2007). Endocytosis optimizes the dynamic localization of membrane proteins that regulate cortical polarity. *Cell* **129**, 411–422.
- Wedlich-Soldner, R., Wai, S.C., Schmidt, T., and Li, R. (2004). Robust cell polarity is a dynamic state established by coupling transport and GTPase signaling. *J. Cell Biol.* **166**, 889–900.
- Slaughter, B.D., Das, A., Schwartz, J.W., Rubinstein, B., and Li, R. (2009). Dual modes of cdc42 recycling fine-tune polarized morphogenesis. *Dev. Cell* **17**, 823–835.
- Adams, A.E.M., and Pringle, J.R. (1984). Relationship of actin and tubulin distribution to bud growth in wild-type and morphogenetic-mutant *Saccharomyces cerevisiae*. *J. Cell Biol.* **98**, 934–945.
- Kilmartin, J.V., and Adams, A.E.M. (1984). Structural rearrangements of tubulin and actin during the cell cycle of the yeast *Saccharomyces*. *J. Cell Biol.* **98**, 922–933.
- Valdez-Taubas, J., and Pelham, H.R. (2003). Slow diffusion of proteins in the yeast plasma membrane allows polarity to be maintained by endocytic cycling. *Curr. Biol.* **13**, 1636–1640.
- Balch, W.E., McCaffery, J.M., Plutner, H., and Farquhar, M.G. (1994). Vesicular stomatitis virus glycoprotein is sorted and concentrated during export from the endoplasmic reticulum. *Cell* **76**, 841–852.
- Bonifacino, J.S., and Traub, L.M. (2003). Signals for sorting of transmembrane proteins to endosomes and lysosomes. *Annu. Rev. Biochem.* **72**, 395–447.
- Sorkin, A. (2004). Cargo recognition during clathrin-mediated endocytosis: A team effort. *Curr. Opin. Cell Biol.* **16**, 392–399.
- Maldonado-Báez, L., and Wendland, B. (2006). Endocytic adaptors: Recruiters, coordinators and regulators. *Trends Cell Biol.* **16**, 505–513.
- Stimpson, H.E., Toret, C.P., Cheng, A.T., Pauly, B.S., and Drubin, D.G. (2009). Early-arriving Syp1p and Ede1p function in endocytic site placement and formation in budding yeast. *Mol. Biol. Cell* **20**, 4640–4651.
- Jenness, D.D., and Spatrick, P. (1986). Down regulation of the alpha-factor pheromone receptor in *S. cerevisiae*. *Cell* **46**, 345–353.
- Rohrer, J., Bénédetti, H., Zanolari, B., and Riezman, H. (1993). Identification of a novel sequence mediating regulated endocytosis of the G protein-coupled alpha-pheromone receptor in yeast. *Mol. Biol. Cell* **4**, 511–521.
- Schandel, K.A., and Jenness, D.D. (1994). Direct evidence for ligand-induced internalization of the yeast alpha-factor pheromone receptor. *Mol. Cell Biol.* **14**, 7245–7255.
- Hicke, L., Zanolari, B., and Riezman, H. (1998). Cytoplasmic tail phosphorylation of the alpha-factor receptor is required for its ubiquitination and internalization. *J. Cell Biol.* **141**, 349–358.
- Toshima, J.Y., Nakanishi, J., Mizuno, K., Toshima, J., and Drubin, D.G. (2009). Requirements for recruitment of a G protein-coupled receptor to clathrin-coated pits in budding yeast. *Mol. Biol. Cell* **20**, 5039–5050.
- Lewis, M.J., Nichols, B.J., Prescianotto-Baschong, C., Riezman, H., and Pelham, H.R. (2000). Specific retrieval of the exocytic SNARE Snc1p from early yeast endosomes. *Mol. Biol. Cell* **11**, 23–38.
- Galan, J.M., Wiederkehr, A., Seol, J.H., Haguenaer-Tsapis, R., Deshaies, R.J., Riezman, H., and Peter, M. (2001). Skp1p and the F-box protein Rcy1p form a non-SCF complex involved in recycling of the SNARE Snc1p in yeast. *Mol. Cell Biol.* **21**, 3105–3117.
- Qiu, W., Neo, S.P., Yu, X., and Cai, M. (2008). A novel septin-associated protein, Syp1p, is required for normal cell cycle-dependent septin cytoskeleton dynamics in yeast. *Genetics* **180**, 1445–1457.
- Gladfelter, A.S., Pringle, J.R., and Lew, D.J. (2001). The septin cortex at the yeast mother-bud neck. *Curr. Opin. Microbiol.* **4**, 681–689.
- Caudron, F., and Barral, Y. (2009). Septins and the lateral compartmentalization of eukaryotic membranes. *Dev. Cell* **16**, 493–506.
- Howell, A.S., Savage, N.S., Johnson, S.A., Bose, I., Wagner, A.W., Zyla, T.R., Nijhout, H.F., Reed, M.C., Goryachev, A.B., and Lew, D.J. (2009). Singularity in polarization: Rewiring yeast cells to make two buds. *Cell* **139**, 731–743.
- Ayscough, K.R., Stryker, J., Pokala, N., Sanders, M., Crews, P., and Drubin, D.G. (1997). High rates of actin filament turnover in budding yeast and roles for actin in establishment and maintenance of cell polarity revealed using the actin inhibitor latrunculin-A. *J. Cell Biol.* **137**, 399–416.
- Kaksonen, M., Sun, Y., and Drubin, D.G. (2003). A pathway for association of receptors, adaptors, and actin during endocytic internalization. *Cell* **115**, 475–487.
- Kaksonen, M., Toret, C.P., and Drubin, D.G. (2006). Harnessing actin dynamics for clathrin-mediated endocytosis. *Nat. Rev. Mol. Cell Biol.* **7**, 404–414.
- Boettner, D.R., D'Agostino, J.L., Torres, O.T., Daugherty-Clarke, K., Uygun, A., Reider, A., Wendland, B., Lemmon, S.K., and Goode, B.L. (2009). The F-BAR protein Syp1 negatively regulates WASp-Arp2/3 complex activity during endocytic patch formation. *Curr. Biol.* **19**, 1979–1987.
- Rodal, A.A., Manning, A.L., Goode, B.L., and Drubin, D.G. (2003). Negative regulation of yeast WASp by two SH3 domain-containing proteins. *Curr. Biol.* **13**, 1000–1008.
- Ehrlich, M., Boll, W., Van Oijen, A., Hariharan, R., Chandran, K., Nibert, M.L., and Kirchhausen, T. (2004). Endocytosis by random initiation and stabilization of clathrin-coated pits. *Cell* **118**, 591–605.
- Loerke, D., Mettlen, M., Yarar, D., Jaqaman, K., Jaqaman, H., Danuser, G., and Schmid, S.L. (2009). Cargo and dynamin regulate clathrin-coated pit maturation. *PLoS Biol.* **7**, e57.
- Novick, P., Field, C., and Schekman, R. (1980). Identification of 23 complementation groups required for post-translational events in the yeast secretory pathway. *Cell* **21**, 205–215.
- Prescianotto-Baschong, C., and Riezman, H. (1998). Morphology of the yeast endocytic pathway. *Mol. Biol. Cell* **9**, 173–189.
- Karpova, T.S., McNally, J.G., Moltz, S.L., and Cooper, J.A. (1998). Assembly and function of the actin cytoskeleton of yeast: Relationships between cables and patches. *J. Cell Biol.* **142**, 1501–1517.
- Bi, E., Chiavetta, J.B., Chen, H., Chen, G.C., Chan, C.S., and Pringle, J.R. (2000). Identification of novel, evolutionarily conserved Cdc42p-interacting proteins and of redundant pathways linking Cdc24p and Cdc42p to actin polarization in yeast. *Mol. Biol. Cell* **11**, 773–793.
- Longtine, M.S., McKenzie, A., 3rd, Demarini, D.J., Shah, N.G., Wach, A., Brachat, A., Philippsen, P., and Pringle, J.R. (1998). Additional modules for versatile and economical PCR-based gene deletion and modification in *Saccharomyces cerevisiae*. *Yeast* **14**, 953–961.
- Kaksonen, M., Toret, C.P., and Drubin, D.G. (2005). A modular design for the clathrin- and actin-mediated endocytosis machinery. *Cell* **123**, 305–320.
- Newpher, T.M., Smith, R.P., Lemmon, V., and Lemmon, S.K. (2005). In vivo dynamics of clathrin and its adaptor-dependent recruitment to the actin-based endocytic machinery in yeast. *Dev. Cell* **9**, 87–98.
- Grigoriev, I., and Akhmanova, A. (2010). Microtubule dynamics at the cell cortex probed by TIRF microscopy. *Methods Cell Biol.* **97**, 91–109.
- Reck-Peterson, S.L., Derr, N.D., and Stuurman, N. (2010). Imaging single molecules using total internal reflection fluorescence microscopy (TIRFM). *Cold Spring Harb Protoc* **2010**, pdb.top73.
- Kim, H.B., Haarer, B.K., and Pringle, J.R. (1991). Cellular morphogenesis in the *Saccharomyces cerevisiae* cell cycle: Localization of the CDC3 gene product and the timing of events at the budding site. *J. Cell Biol.* **112**, 535–544.